Controlling Rotation of 2D Material Flakes

Shuze Zhu[1]*, Pascal Pochet[2]*, Harley T. Johnson[1]*

[1]Department of Mechanical Science and Engineering, University of Illinois at Urbana-Champaign, Urbana, IL 61801, USA

[2]Laboratory of Atomistic Simulation (L_Sim), Univ. Grenoble Alpes & CEA 38054 Grenoble, FRANCE

Email of corresponding authors*:

Shuze Zhu (shuzezhu@illinois.edu); Pascal Pochet (pascal.pochet@cea.fr); Harley T. Johnson (htj@illinois.edu)

ABSTRACT: Interlayer rotational alignment in vdW structures of two-dimensional materials couples strongly to electronic properties and, therefore, has significant technological implications. Nevertheless, controlling rotation of an arbitrary two-dimensional material flake remains a challenge in the development of rotation-tunable electronics, for the emerging field of twistronics. In this article, we reveal a general moiré-driven mechanism that governs the interlayer rotation. Controlling the moiré can therefore hold promise for controlling interlayer rotation. We further demonstrate mismatch strain engineering as a useful tool to design the interlayer rotation *via* changing the energy landscape of moiré within a finite-sized region. The robustness and programmable nature of our approach arise from moiré symmetry, energetics, and mechanics. Our approach provides another possibilities to the on-demand design of rotation-tunable electronics.

KEYWORDS: two-dimensional materials, moiré, interlayer rotation, strain engineering

Van der Waals (vdW) structures of two-dimensional (2D) materials possess significant potential for studying fundamental properties and developing exotic nanoscale technologies.[1, 2] In such material systems, the relative interlayer rotation between layers of 2D materials is a commonly observed feature. For example, the triangle-shaped nucleated domains of MoS_2 bilayers grown by chemical vapour deposition (CVD) usually have several discrete interlayer rotation angles (Figure 1(a));[3, 4] a similar observation has been made in other 2D material bilayer systems.[2] It is well known that the interlayer rotation changes interlayer coupling, leading to modulation of electronic structures, and tremendous potential for tuning the electronic properties.[4-16] For example, the photoluminescence spectra of MoS_2 bilayers grown by CVD are clearly shown to be dependent on rotation.[3, 4] In fact, a small variation in interlayer rotation is able to induce huge variation in electronic structures. For example, superconducting states in bilayer graphene have been observed after imposing a small interlayer rotation of 1.1 degree.[6] Recently, a dynamically rotatable electronic device architecture was used to demonstrate significant electronic property variations due to rotations of just a few degrees.[9] Until now, a fundamental understanding of interlayer rotation effects has remained elusive, posing significant challenges to realizing the full potential of electronic applications in 2D materials. For example, it has not been explained why, during CVD growth of 2D layers, there is such a wide range of rotation angles of nucleated domains, leading to significant grain boundary formation. This limited understanding also adds to the difficulty of rational design of functional structures and devices at extreme length scales. For example, existing methods of fine tuning of interlayer rotation (*e.g.*, using an AFM tip[9] to push) inevitably suffer from experimental limitations in the nanoscale regime (*e.g.*,

in fabricating nanoscale devices and manipulating nanoscale objects). Such lack of control is undesirable for nanoscale twistronics.[8, 9] So how can one design rotatable electronics at the nanoscale? How can interlayer rotation of nanoscale nucleated domains be manipulated during CVD growth? The answers to these questions depend upon a mechanistic understanding of the driving force behind interlayer rotation in 2D layers.

In this article, we reveal a general moiré-driven mechanism that governs the interlayer rotation in 2D layers, using bilayer MoS_2 and graphene as examples. This moiré-driven mechanism extends our moiré engineering concept[17] and is generalizable to various 2D materials, in which interlayer rotation between the layers is governed by a periodic variation of atomic registry at the interface, giving rise to a moiré pattern with a well-defined periodicity.[18] We find that it is the interface lattice moiré that governs the interlayer rotation. Given the significance of the coupling between electronic structure and interlayer rotation in 2D layers, our findings offer another possibilities to the on-demand design of rotation-tunable electronics.

RESULTS AND DISCUSSION

Figure 1(b) describes the central question of interest in this article. In a 2D bilayer system in which the top layer takes the shape of an equilateral triangle (motivated by experimental observations such as those in Figure 1(a)), what is the relationship between the preferred rotational orientation and the flake size?

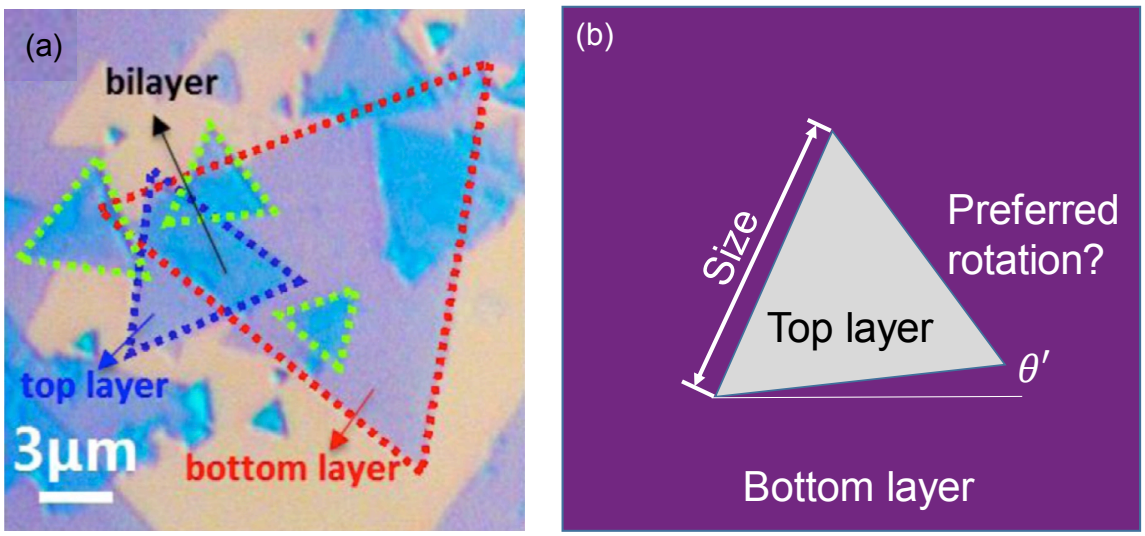

Figure 1. (a) Triangle-shaped nucleated domains of MoS_2 bilayers grown by chemical vapour deposition (CVD). Many interlayer rotation angles can be observed.[4] This imaged is adapted with permission from ref 4. Copyright 2014 American Chemical Society. (b) In a 2D bilayer system, how does the preferred rotational orientation relate to the flake size?

We first use molecular dynamics (MD) simulations to demonstrate rotational behavior with atomistic resolution. Figure 2(a) and Figure 2(b) describe the MD model, which consists of two MoS_2 layers. For the purpose of demonstration, the top layer is modeled as a triangular flake with side length 10.825 nm (Figure 2(b)). To stack these two layer together (Figure 2(a)), one must specify a certain initial stacking pattern. Here three representative initial stacking patterns are considered, namely AA, 3R and 2H, following the conventional notation of high-symmetry stacking in bilayer MoS_2.[19] These stacking patterns are chosen since they cover both the highest energy stacking (AA) and the lowest energy stacking (3R and 2H). The MD simulation proceeds as follows: for a given initial

stacking pattern, an initial rotation is first imposed counterclockwise (Figure 2(c)), and then changes in the rotation angle are monitored during structural relaxation (See Section 1 in supporting information). The MoS_2 MD simulation is carried out in LAMMPS[20] using the ReaxFF reactive force field,[21] which is based on quantum mechanical simulations and has shown favorable comparison with first-principles data in terms of mechanical and morphological properties.[21] The energy in ReaxFF includes the nonbonded van der Waals (vdW) interaction in the form of a distance-corrected Morse-potential.[21, 22] Figure 2(c) shows the MD simulation results. The top row shows the initial stacked and rotated, unrelaxed configurations; the bottom row shows the relaxed configurations from MD simulations. All of the atoms in the top layer triangular flake are colored white for visual clarity. Quantitative assessment of the rotation angle in Figure 2(c) is done in the framework of continuum mechanics (See Section 1 in supporting information). For the AA stacking, we find that, if the initial unrelaxed rotation angle is 1 degree, for example, the relaxed rotation angle appears to be more than 1 degree; in other words, the rotation in the counterclockwise direction continues during relaxation. If the initial unrelaxed rotation angle is 6 degrees, for example, the relaxed rotation angle appears to be unchanged. By comparison, we can see that the initial rotation angle matters. For the 3R stacking, if the initial unrelaxed rotation angle is 2 degrees, for example, the relaxation does not show the same rotation direction as seen in AA stacking. The rotation direction reverses, and the relaxed rotation angle is zero, completely back to the initial 3R stacking. If the initial unrelaxed rotation angle is 3.5 degrees, however, the relaxed rotation angle appears to be unchanged. The rotation behavior for the 2H stacking is almost the same as that of the 3R stacking. For example, for 2 degree initial unrelaxed

rotation angle, the relaxed rotation angle is zero. For 3 degree initial unrelaxed rotation angle, the relaxed rotation angle appears to be unchanged. In view of all these results, it is apparent that both the initial stacking and initial rotation angle play a role, and that there might be multiple stable minimum energy configurations.

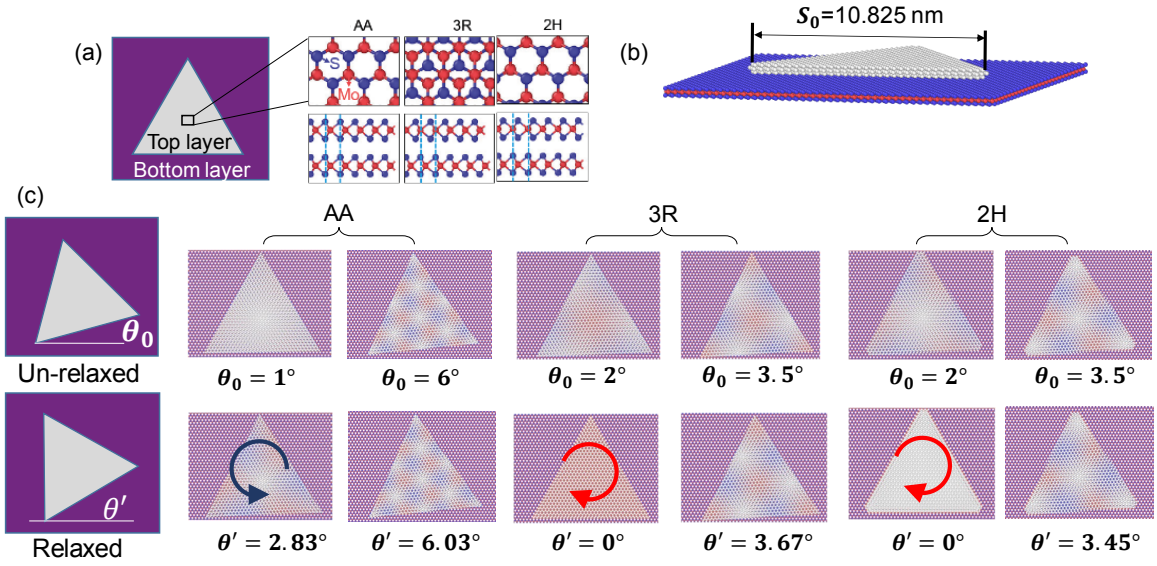

Figure 2. (a) schematic showing the MD simulation model, in which a triangular top layer is placed on a large bottom layer. Three initial stacking patterns of MoS_2 are studied in MD simulations. (b) perspective view of the atomistic model of the MoS_2 bilayer. (c) MD simulation results. The top row shows the initial stacked and rotated, unrelaxed configurations; the bottom row shows the relaxed configurations from MD simulations.

In order to develop a simple understanding of interlayer rotation that can be applied even at the largest scales, we adopt a generic model that we have described in recent work,[18] and which we refer to here as the interface lattice model (ILM) (Figure 3(a)). The assumption of this model, motivated by the results of the MD simulations (Figure 2(c)), is

that interfacial interactions dominate, so only the two atomic layers at the interface are considered, while neglecting all other atoms. The nature of the ILM requires identifying the interfacial stacking pattern in the full atomistic model (See Section 2 in supporting information). In our case, the AA stacking in the full atomistic model corresponds to a unique interfacial stacking, while both 3R and 2H stacking share the same interfacial stacking type, which is equivalent to AB stacking. Indeed, because the same interfacial stacking is shared for both 3R and 2H stacking, the ILM predicts that the same rotation behavior is shared for both 3R and 2H stacking. We then consider the relationship between interfacial energy and imposed rotation angle using ILM; the calculation results are shown in Figure 3(b). In addition to the flake size as shown in Figure 2, in order to explore the effect of flake size, larger and smaller flake sizes (2x and 0.5x, respectively) are also considered. The horizontal axis is the rotation angle, the vertical axis is the energy. An immediate observation is that the stacking and size are related. In the case of AA stacking, the energy is maximum at zero rotation, while in the AB stacking, the energy is minimum at zero rotation. In addition, increasing the flake size shifts the location of each of the multiple energy minima or maxima toward zero. This observation explains growth processes in which interlayer rotation of flakes are seen to have a diverse distribution, because the energy landscape continually changes with respect to flake size. To allow a direct comparison between the ILM calculation results and the full MD simulations, we label the rotation angles on the curve corresponding to the case shown in Figure 2(c). Examining the location of the nearest local energy minimum for each angle explains the fully atomistic simulation results. For example, for AA stacking, the initial one degree rotation angle would relax to 2.83 degrees in the MD simulation, which

corresponds to the first local energy minimum predicted from the ILM. For 3R and 2H stacking, the initial 3.5 degree rotation angle is already near to the region of the first local energy minimum, and therefore no significant global rotation is observed. The good agreement between ILM and full MD confirms that the interface interaction dominates the rotation behavior.

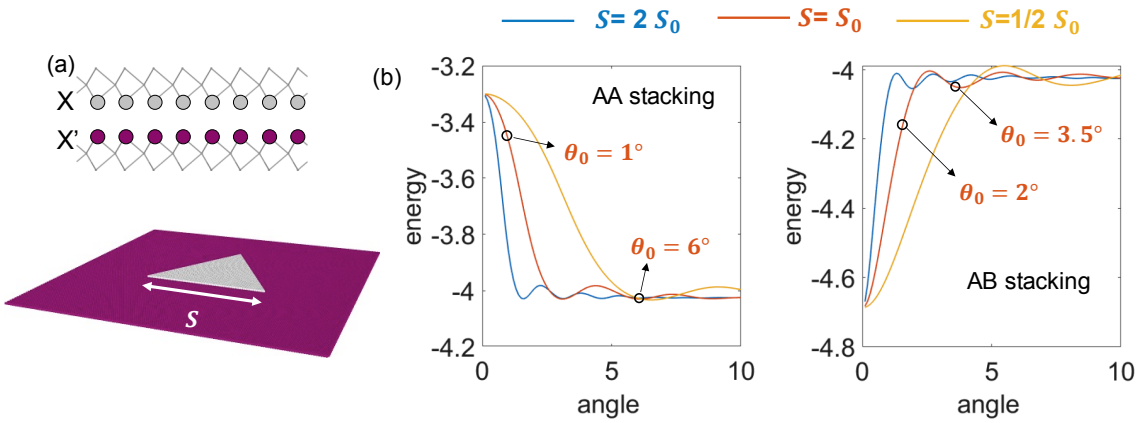

Figure 3. (a) schematic showing the interface lattice model (ILM), where only the atomic layers at the interface are considered. (b) energy-angle curves from the ILM calculation, for three flake sizes and two interface stacking variants. The labeled angles correspond to the MD simulation shown in Figure 2.

Although the ILM can explain well the rotation behavior, it does not offer a clear physical explanation for the energy landscape during rotation. However, the MD simulation reveals that the moiré patterns are rotation-dependent (see Figure 2), which motivates us to further investigate the correlation of rotation behavior to the interface lattice moiré pattern. Figure 4(a) and 4(b) show the obtained interface lattice moiré pattern (See Section 3 in supporting information) for the sets of angles investigated above.

The red colored region corresponds to the high energy stacking domain, while the blue colored region denotes the low energy stacking domain. Obviously, the interface lattice moiré is dependent on the interlayer rotation (*e.g.*, the spacing between the high energy domains decreases as rotation angle increases). In fact, both the orientation and wavelength of the moiré are dependent on the rotation.[23] Close inspection shows that each high energy domain is surrounded by six low energy domains, and each low energy domain is surrounded by three high energy domains. There are also transitional domains between high energy domains and low energy domains.[18] In addition, whether the high energy domain or the low energy domain occupies the center of the triangle depends on the initial stacking. The interfacial AA stacking is associated with the high energy center (Figure 4(a)) while the AB stacking is associated with the low energy center (Figure 4(b)).

We find that the addition of rows of moiré spots, as rotation increases, is responsible for the quasi-periodic nature of the energy curve (separating energy minima or maxima). Taking the interfacial AA stacking as an example, the local minima are reached when the edges of the triangular shape cut through the centers of the high-energy domains (colored in red in Figure 4(a)). In such configurations, the area percentage of the low-energy domains (colored in blue in Figure 4(a)) is maximized. The observation is slightly different in the case of the interfacial AB stacking. The local maxima are reached when the edges of the triangular shape cut through the centers of the high-energy domains (colored in red in Figure 4(b)). In such configurations, the area percentage of the low-energy domains (colored in blue in Figure 4(b)) is minimized. The above contrast in energy evolution is apparently related to the type of energy domain at the center of the triangle.

These observations further motivate us to correlate the interface lattice moiré patterns to the energy landscape during the rotation. We introduce another level of description that we describe as a moiré domain model (MDM) (Figure 4(c)) (See Section 4 in supporting information). Both high energy domains and low energy domains are represented by circular disks tangential to each other. For a given triangle (representing the top triangle flake), the MDM energy landscape is calculated by summing up the energies of evolving regions of the disks within that triangle at a given flake rotation. The geometrical distribution of these disks at a given rotation can be predetermined.[23] For example, the spacing between the centers of high energy domains is a function of the rotation (Figure 4(c)). Figure 4(d) shows good agreement between the angles of the local energy maxima or minima computed *via* ILM or MDM, for one triangle size (See Section 5 in supporting information for other sizes). The extremum index is counted in the angle ascending direction (excluding zero). For example, for the interfacial AA stacking, the first extremum corresponds to the first local energy minimum, while for the interfacial AB stacking, the first extremum corresponds to the first local energy maximum. The striking agreement of the MDM location of the energy extrema with those from the ILM (Figure 3(b)), indicates that the rotation is fundamentally driven by interface lattice moiré.

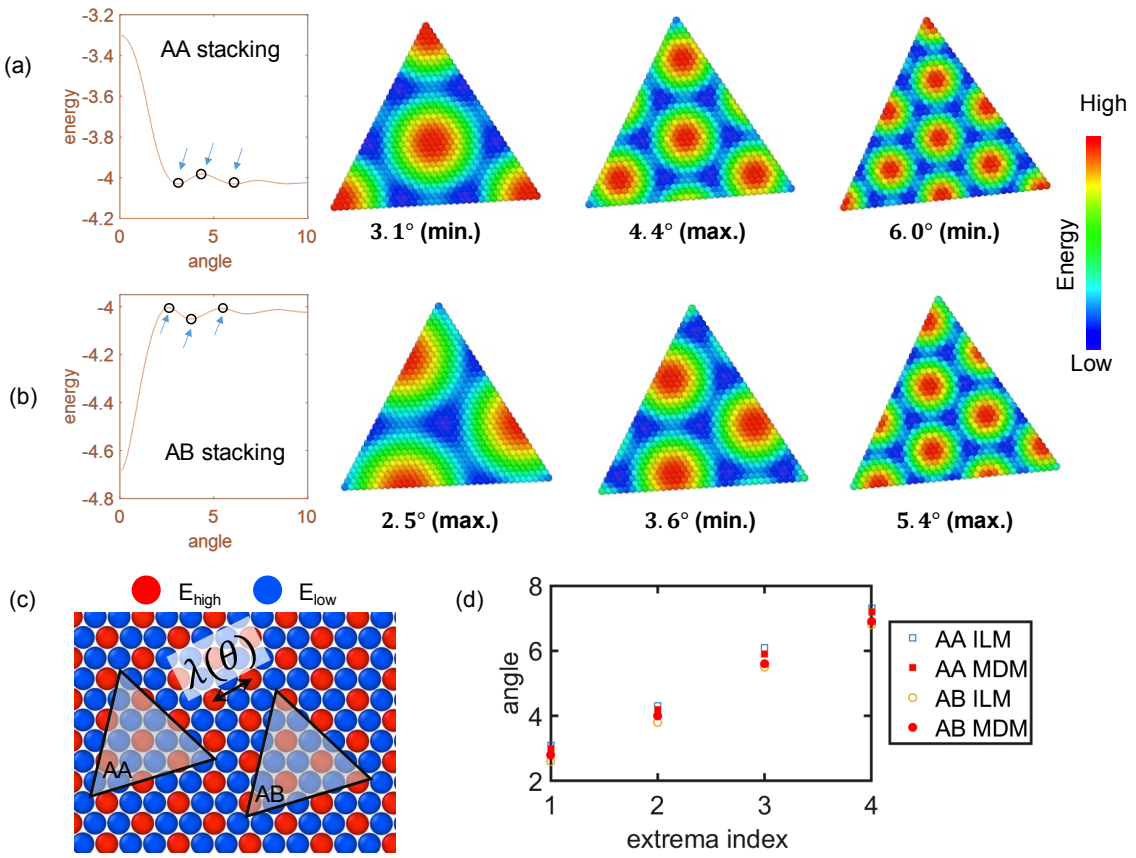

Figure 4. (a) evolution of interface lattice moiré for interfacial AA stacking from the ILM calculation. Three sequential local extremum configurations are displayed. Their corresponding locations on the energy-angle curve are indicated by arrows. Color coding highlights the domain energy difference. The flake size is the same as in Figure 2. (b) similar to (a) but for interfacial AB stacking. (c) Schematic of the moiré domain model (MDM). For a given triangle (representing the top triangle flake), the MDM energy landscape is calculated by summing up the energies of evolving regions of the disks within that triangle at a given rotation. The center of the triangle for AA stacking is high energy while that for AB stacking is low energy. (d) Agreement between MDM and ILM in terms of the angles of local maximum or minimum.

The analysis above establishes that the interlayer rotation is driven by the interface lattice moiré. This fundamental principle is universal for all types and all sizes of 2D layers because the interface lattice moiré is intrinsic to any Van der Waals heterostructure. The general applicability is purely based on geometry. As long as moiré patterns are formed between two layers of 2D materials with the hexagonal lattice, the high-energy stacking domains will be in a triangular array, and the low-energy domains will be in a hexagonal array (See Figure S6 in supporting information). This geometrical similarity of the moiré patterns formed between 2D materials guarantees the general applicability of our theory. We can expect that, although the sets of data shown so far are calculated for triangular MoS_2 flakes, the same data are quantitatively valid for any triangular 2D material flakes if the geometrical similarity is met. That is, for different 2D material systems where the ratio of the triangular flake size to its lattice constant is the same, the rotation behavior will be, in general, the same. To concretely demonstrate this point, we performed parallel simulations for bilayer graphene (See Figure S7 and S8 in supporting information). It is found that the rotation behavior of geometrically-similar graphene systems displays stunning quantitative agreement with that of the MoS_2 system. As a result of such general applicability, it can be further deduced that for 2D material systems where the ratio of the triangular flake size to its lattice constant is the same, the set of rotation angles for local energy extremes will be, in general, the same.

Therefore, controlling the interface lattice moiré could lead to control of the interlayer rotation, offering another possibilities for rotation-tunable electronics, or twistronics. In principle, the moiré might be controlled using strain (Figure 5(a)) as a control parameter, since mismatch strain between layers also induces a moiré pattern. Thanks to techniques

for applying large elastic deformation, and the capacity of substrate materials to sustain large elastic deformation, strain engineering is an effective tool to tune the electronic signatures of 2D materials. For example, elastic tensile strains as large as 10% have shown promising applications in engineering band gaps in graphene[24] and transition-metal dichalcogenides (TMDs).[25] By manipulating the relative mismatch between layers, the moiré pattern could be changed, which could lead to spontaneous rotations in response to the energy landscapes described above. We consider a bilayer system placed (or grown) on a stretchable substrate, and we consider the possibility that by straining the bottom layer along with the substrate, one may guide the rotation of the top flake. We assume that the isolated top flake is not subjected to significant strain due to the interaction with the substrate. This may be justified in several ways: first, the in-plane stiffness of the 2D material (resulting from covalent bonding) is typically orders of magnitude larger than that associated with the non-bonding interaction. Furthermore, the existence of the bottom layer itself separates the top layer from the substrate by a distance of more than 0.7 nm, where the non-bonding interactions are expected to have decayed to near zero. Second, one may intentionally place the top flake on a portion of the bottom layer that is suspended over pits or channels in the substrate, so that the top flake does not interact with the substrate at all, but instead with only the strained bottom layer. In either scenario, we assume that our proposed principles apply, just as if the bottom layer was stretched by gripping it at its remote edges, far from the top flake. We also want to emphasize that this scenario of imposing mismatch strain naturally extends to van der Waals hetero-layers, where the intrinsic lattice mismatch plays the role of strain. Next we

examine the energy landscape in the parameter space of strain and interlayer rotation using our computational framework and atomistic simulations.

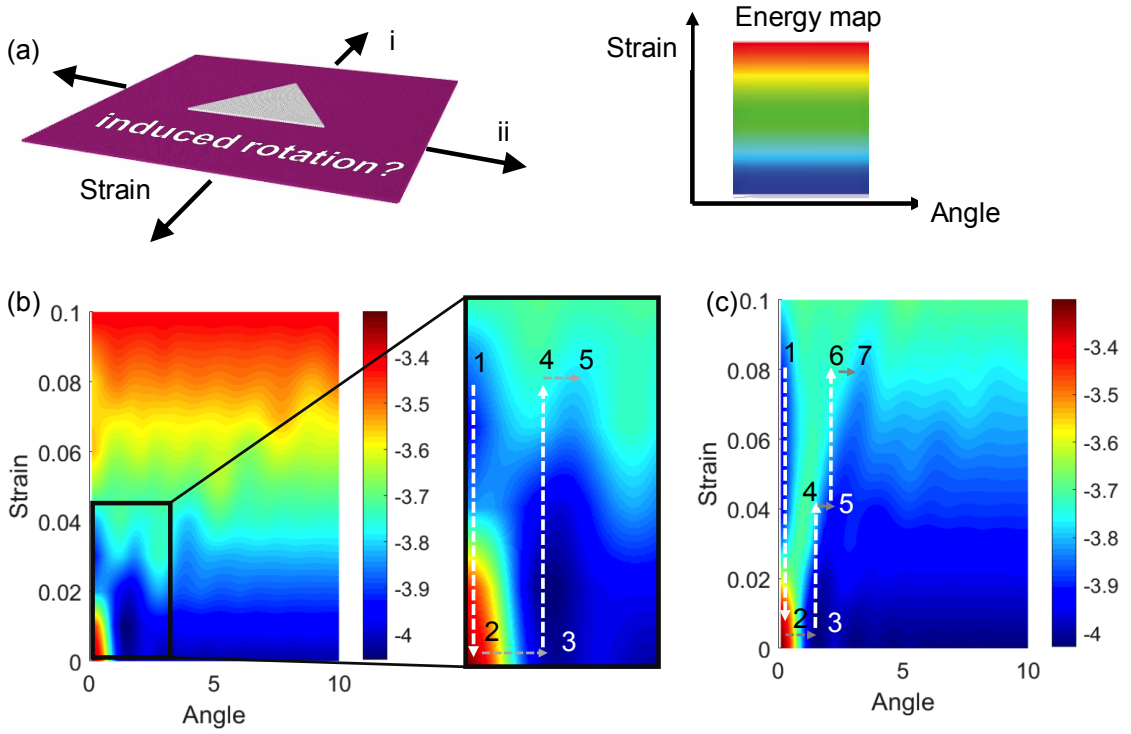

Figure 5. (a) schematic showing the concept of strain-induced interlayer rotation, and the energy map in the space of imposed strain and rotation angle that can guide the rational design. (b) energy map for biaxial tensile strain, acting on the bottom layer. This is for flake size that is twice that of Figure 2. Zoomed energy map showing five labeled states that are connected by an imposed strain path (dashed white arrow) and relaxation path (dashed gray arrow). The imposed strain path drives state #1 to state #2, and state #3 to state #4. The system relaxes spontaneously from state #2 to state #3, and from state #4 to state #5. (c) energy map and paths to tune rotation angle in uniaxial strain condition for the same system of Figure 5(b). The strain is along the (i) direction in Figure 5(a).

Figure 5(b) shows an energy map for biaxial tensile strain applied to the bottom layer. This map is computed using the ILM for bilayer MoS_2, while it is also quantitatively valid for a geometrically-similar bilayer graphene (see Section 7 in supporting information), further demonstrating the robustness of our theory. The vertical axis denotes the imposed biaxial strain (up to 10%) on the bottom layer, while the horizontal axis denotes the interlayer rotation angle (up to 10 degrees). Thus, for imposed biaxial strain as a tuning input, the map shows the energy of the bilayer system at any interlayer rotation, which allows us to identify the paths to achieve interlayer rotation that renders the minimum energy of the system. For example, in the magnified energy map there are five states labeled. If the bilayer system starts from state #1, reducing the biaxial strain under fixed rotation drives up the energy of the system as it approaches state #2. If allowed to rotate, the system would then spontaneously relax to state #3. At this stage, increasing the biaxial strain then increases the energy of the system to state #4, from which it can spontaneously rotate and relax to state #5. At this point, by controlling only the strain in the substrate, the interlayer rotation angle has increased about 2 degrees (see Figure S11 in supporting information). Figure 5(c) shows the energy map for the same system that is studied in Figure 5(b) using only uniaxial strain along the (i) direction (shown in Figure 5(a)), since under certain conditions uniaxial strain might be easier to implement. In this case it is also possible to identify a seven-state path that can be connected *via* strain tuning and rotational relaxation. In this case, the interlayer rotation angle changes more than 3 degrees (see Figure S12 in supporting information). These changes of a few degree in interlayer rotation would already be sufficient to induce significant changes in electronic structure.[6, 9] To best interpret the paths, one can think of

a combined transition vector that is the sum of an applied strain path vector (white dashed arrow) and a relaxation angle path vector (grey dashed arrow). This combined transition vector tells the location of the final state of the relaxed system after a particular magnitude of strain change is imposed. For practical applications, we note that the range of possible experimental strain rates is typically many orders of magnitudes lower than is accessible in atomistic simulations. Thus, the quasi-static strain change is more relevant, which would correspond to the infinite-state path with infinitesimal straining-relaxation step, best characterized by the concept of the combined transition vector. The sequential path of applied strain followed by relaxation angle would apply strictly only in the limit of very high strain rate.

We note a few other interesting implications of these energy maps. For example, we find that the energy map evolves as the size of the triangular flake increases (see Section 9 in supporting information), which has implications for the growth process. A state which is at a local energy minimum for a certain size may not remain stable if the size increases (*e.g.*, by growth). As a result, the growing flake might rotate to new stable configurations according to gradients in the energy map. Given that the growth speed of different nucleated domains may vary considerably due to local conditions, the distribution of triangular domain sizes might not be expected to remain uniform (*e.g.*, Figure 1(a)), and therefore their varying rates of interlayer rotation eventually could lead to orientation mismatch[26] and the formation of grain boundaries.[27, 28] Such an argument should be in principle applicable in other 2D material bilayer systems. In fact, a quantitative calculation (Figure S16) using our current analysis can explain very well the experimental observed distribution of rotation angle of $MoSe_2$ grown on graphene in a

recent report,[29] further demonstrating the interest of the method described in current study for growth processes.

Another interesting possibility is that while strain may be used to tune the interlayer rotation angle, it may also be possible to use the interlayer rotation to tune the mismatch strain. In this case, the tuning pathways in Figure 5(b) are reversed. For example, if the system is at state #3, reducing the interlayer rotation will drive the system up to state #2, and then the strain relaxation path would lead the system spontaneously to state #1, by either inducing tensile strain in the bottom layer, or by inducing compressive strain in the top triangle layer, in order to achieve the corresponding mismatch strain (about 0.03 for the state #1 as shown in Figure 5(b)). We suggest that imposing the interlayer rotation of the top flake might be possible using an AFM tip[9] on a micrometer-sized system.

CONCLUSION

In conclusion, in this article we reveal a fundamental mechanical principle of interlayer rotation in layered systems of 2D materials. We find that the moiré is the governing factor for the interlayer rotation. The preferred interlayer rotation minimizes the total energy of the moiré domains confined in a finite-sized region. Thus, controlling the moiré will make it possible to control interlayer rotation. We further demonstrate that strain can be used to control the interlayer rotation. Our findings add to the fundamental understanding of interface mechanics in 2D material systems and suggest a strategy for designing nanoscale rotation-tunable electronics.

METHOD/EXPERIMENTAL SECTION

The structural relaxation in MD simulation (Figure 2) as well as in interface lattice model (ILM, Figure 3) is carried out using the conjugate gradient (CG) algorithm followed by Hessian-free truncated Newton algorithm until either the total energy change between successive iterations divided by the energy magnitude is less than or equal to 10^{-20} or the total force is less than 10^{-15} eVÅ^{-1}. The moiré domain model (Figure 4) is a pure geometry model. The total energy within the area of the triangle is calculated by summing up the energies of the evolving area of the circles within that triangle boundary (including partial circles that are cut by the boundary, and the transitional area) at a given flake rotation. Further detailed description of computational methods can be found in Supporting Information.

SUPPORTING INFORMATION

The Supporting Information is available free of charge on the ACS Publications website at DOI:

Additional figures are included in the following sections of the Supporting Information. Section 1 describes the MD relaxation process and the characterization of rotation angle; Section 2 describes interfacial stacking of the atomistic structure; Section 3 describes the interfacial lattice model set up; Section 4 describes the moiré domain model set up; Section 5 compares the interfacial lattice model and the moiré domain model; Section 6 addresses the general applicability of the model; Section 7 presents energy maps; Section 8 compares the $MoSe_2$/graphene system with experimental data; Section 9 describes evolving energy landscapes during growth.

ACKNOWLEDGEMENT

The authors gratefully acknowledge the support of the Army Research Office (W911NF-17-1-0544) Material Science Division under Dr. Chakrapani Varanasi. The partial support of NSF grant number CMMI 18-25300 (MOMS program) is also acknowledged.

REFERENCES

1. Novoselov, K.; Mishchenko, A.; Carvalho, A.; Neto, A. 2D Materials and van der Waals Heterostructures. *Science* **2016**, *353*, aac9439.
2. Geim, A.; Grigorieva, I. Van der Waals Heterostructures. *Nature* **2013**, *499*, 419-425.
3. Liu, K.; Zhang, L.; Cao, T.; Jin, C.; Qiu, D.; Zhou, Q.; Zettl, A.; Yang, P.; Louie, S.; Wang, F. Evolution of Interlayer Coupling in Twisted Molybdenum Disulfide Bilayers. *Nat. Commun.* **2014**, *5, 4966*.
4. Huang, S.; Ling, X.; Liang, L.; Kong, J.; Terrones, H.; Meunier, V.; Dresselhaus, M. Probing the Interlayer Coupling of Twisted Bilayer MoS2 Using Photoluminescence Spectroscopy. *Nano Lett.* **2014**, *14*, 5500-5508.
5. Wang, Y.; Wang, Z.; Yao, W.; Liu, G.; Yu, H. Interlayer Coupling in Commensurate and Incommensurate Bilayer Structures of Transition-Metal Dichalcogenides. *Phys. Rev. B: Condens. Matter Mater. Phys.* **2017**, *95*, 115429.
6. Cao, Y.; Fatemi, V.; Fang, S.; Watanabe, K.; Taniguchi, T.; Kaxiras, E.; Jarillo-Herrero, P. Unconventional Superconductivity in Magic-Angle Graphene Superlattices. *Nature* **2018**, *556*, 43-50.
7. Wang, K.; Huang, B.; Tian, M.; Ceballos, F.; Lin, M.; Mahjouri-Samani, M.; Boulesbaa, A.; Puretzky, A.; Rouleau, C.; Yoon, M.; Zhao, H.; Xiao, K.; Duscher, G.; Geohegan, D. Interlayer Coupling in Twisted WSe2/WS2 Bilayer Heterostructures Revealed by Optical Spectroscopy. *ACS Nano* **2016**, *10*, 6612-6622.
8. Carr, S.; Massatt, D.; Fang, S.; Cazeaux, P.; Luskin, M.; Kaxiras, E. Twistronics: Manipulating the Electronic Properties of Two-Dimensional Layered Structures Through Their Twist Angle. *Phys. Rev. B: Condens. Matter Mater. Phys.* **2017**, *95*, 075420.
9. Ribeiro-Palau, R.; Zhang, C.; Watanabe, K.; Taniguchi, T.; Hone, J.; Dean, C. Twistable Electronics with Dynamically Rotatable Heterostructures. *Science* **2018**, *361*, 690-693.
10. Wu, M.; Qian, X.; Li, J. Tunable Exciton Funnel Using Moire Super lattice in Twisted van der Waals Bilayer. *Nano Lett.* **2014**, *14*, 5350-5357.
11. Hunt, B.; Sanchez-Yamagishi, J.; Young, A.; Yankowitz, M.; LeRoy, B.; Watanabe, K.; Taniguchi, T.; Moon, P.; Koshino, M.; Jarillo-Herrero, P.; Ashoori, R. Massive Dirac Fermions and Hofstadter Butterfly in a van der Waals Heterostructure. *Science* **2013**, *340*, 1427-1430.
12. Ponomarenko, L.; Gorbachev, R.; Yu, G.; Elias, D.; Jalil, R.; Patel, A.; Mishchenko, A.; Mayorov, A.; Woods, C.; Wallbank, J.; Mucha-Kruczynski, M.; Piot, B.; Potemski, M.; Grigorieva, I.; Novoselov, K.; Guinea, F.; Fal'ko, V.; Geim, A. Cloning of Dirac Fermions in Graphene Superlattices. *Nature* **2013**, *497* , 594-597.
13. Dean, C.; Wang, L.; Maher, P.; Forsythe, C.; Ghahari, F.; Gao, Y.; Katoch, J.; Ishigami, M.; Moon, P.; Koshino, M.; Taniguchi, T.; Watanabe, K.; Shepard, K.; Hone, J.;

Kim, P. Hofstadter's Butterfly and the Fractal Quantum Hall Effect in Moire Superlattices. *Nature* **2013**, *497*, 598-602.
14. Gorbachev, R.; Song, J.; Yu, G.; Kretinin, A.; Withers, F.; Cao, Y.; Mishchenko, A.; Grigorieva, I.; Novoselov, K.; Levitov, L.; Geim, A. Detecting Topological Currents in Graphene Superlattices. *Science* **2014**, *346*, 448-451.
15. Wu, F.; Lovorn, T.; MacDonald, A. Topological Exciton Bands in Moire Heterojunctions. *Phys. Rev. Lett.* **2017**, *118*, 147401.
16. Tong, Q.; Yu, H.; Zhu, Q.; Wang, Y.; Xu, X.; Yao, A. Topological Mosaics in Moire Superlattices of van der Waals Heterobilayers. *Nat. Phys.* **2017**, *13*, 356-362.
17. Pochet, P.; McGuigan, B.; Coraux, J.; Johnson, H. Toward Moire Engineering in 2D Materials *via* Dislocation Theory. *Appl. Mater. Today* **2017**, *9*, 240-250.
18. Zhu, S.; Johnson, H. Moire-Templated Strain Patterning in Transition-Metal Dichalcogenides and Application in Twisted Bilayer MoS_2. *Nanoscale* **2018**, *10*, 20689-20701.
19. Huang, S.; Liang, L.; Ling, X.; Puretzky, A.; Geohegan, D.; Sumpter, B.; Kong, J.; Meunier, V.; Dresselhaus, M. Low-Frequency Interlayer Raman Modes to Probe Interface of Twisted Bilayer MoS2. *Nano Lett.* **2016**, *16*, 1435-1444.
20. Plimpton, S. Fast Parallel Algorithms for Short-Range Molecular-Dynamics. *J. Comput. Phys.* **1995,** *117*, 1-19.
21. Ostadhossein, A.; Rahnamoun, A.; Wang, Y.; Zhao, P.; Zhang, S.; Crespi, V.; van Duin, A. ReaxFF Reactive Force-Field Study of Molybdenum Disulfide (MoS2). *J. Phys. Chem. Lett.* **2017**, *8*, 631-640.
22. van Duin, A.; Dasgupta, S.; Lorant, F.; Goddard, W. ReaxFF: A Reactive Force Field for Hydrocarbons. *J. Phys. Chem. A* **2001**, *105*, 9396-9409.
23. Hermann, K. Periodic Overlayers and Moire Patterns: Theoretical Studies of Geometric Properties. *J. Phys.: Condens. Matter* **2012**, *24*, 314210.
24. Zhu, S.; Stroscio, J.; Li, T. Programmable Extreme Pseudomagnetic Fields in Graphene by a Uniaxial Stretch. *Phys. Rev. Lett.* **2015**, *115*, 245501.
25. Feng, J.; Qian, X.; Huang, C.; Li, J. Strain-Engineered Artificial Atom as a Broad-Spectrum Solar Energy Funnel. *Nat. Photonics* **2012**, *6*, 865-871.
26. Han, G.; Kybert, N.; Naylor, C.; Lee, B.; Ping, J.; Park, J.; Kang, J.; Lee, S.; Lee, Y.; Agarwal, R.; Johnson, A. Seeded Growth of Highly Crystalline Molybdenum Disulphide Monolayers at Controlled Locations. *Nat. Commun.* **2015**, *6, 6128*.
27. van der Zande, A.; Huang, P.; Chenet, D.; Berkelbach, T.; You, Y.; Lee, G.; Heinz, T.; Reichman, D.; Muller, D.; Hone, J. Grains and Grain Boundaries in Highly Crystalline Monolayer Molybdenum Disulphide. *Nat. Mater.* **2013**, *12*, 554-561.
28. Najmaei, S.; Liu, Z.; Zhou, W.; Zou, X.; Shi, G.; Lei, S.; Yakobson, B.; Idrobo, J.; Ajayan, P.; Lou, J. Vapour Phase Growth and Grain Boundary Structure of Molybdenum Disulphide Atomic Layers. *Nat. Mater.* **2013**, *12*, 754-759.
29. Alvarez, C.; Dau, M.; Marty, A.; Vergnaud, C.; Le Poche, H.; Pochet, P.; Jamet, M.; Okuno, H. Impact of a van der Waals Interface on Intrinsic and Extrinsic Defects in an MoSe2 Monolayer. *Nanotechnology* **2018**, *29*, 425706.

Table of content